ELECTRICAL ENGINEERING

Discovery of true electrochemical reactions for ultrahigh catalyst mass activity in water splitting

Jingke Mo,[1] Zhenye Kang,[1] Scott T. Retterer,[2] David A. Cullen,[2] Todd J. Toops,[2] Johney B. Green Jr.,[3] Matthew M. Mench,[4] Feng-Yuan Zhang[1]*

Better understanding of true electrochemical reaction behaviors in electrochemical energy devices has long been desired. It has been assumed so far that the reactions occur across the entire catalyst layer (CL), which is designed and fabricated uniformly with catalysts, conductors of protons and electrons, and pathways for reactants and products. By introducing a state-of-the-art characterization system, a thin, highly tunable liquid/gas diffusion layer (LGDL), and an innovative design of electrochemical proton exchange membrane electrolyzer cells (PEMECs), the electrochemical reactions on both microspatial and microtemporal scales are revealed for the first time. Surprisingly, reactions occur only on the CL adjacent to good electrical conductors. On the basis of these findings, new CL fabrications on the novel LGDLs exhibit more than 50 times higher mass activity than conventional catalyst-coated membranes in PEMECs. This discovery presents an opportunity to enhance the multiphase interfacial effects, maximizing the use of the catalysts and significantly reducing the cost of these devices.

INTRODUCTION

The demand for energy has increased rapidly over the past few decades as a result of worldwide economic growth, population expansion, and industrialization. Meeting this demand can be difficult and often results in high levels of pollution and greenhouse gas emissions, creating serious health and environmental concerns and elevating indirect costs to society. More recently, there has been a shift to renewable technologies, such as hydro, wind, and solar technologies, for power generation. However, intermittent power disruptions are common when relying purely on renewable resources. This occurs where there is a mismatch between the energy generated and demand. Energy storage eases intermittent power disruptions by storing the excess power generated by renewable resources during periods of low demand and distributing the power during periods of heightened demand. This helps balance the load and reduce reliance on nonrenewable resources. Hydrogen, a high–specific energy, environmentally friendly fuel, is expected to be one of the most promising energy carriers in the near future (*1*–*9*). Water electrolysis, splitting water into hydrogen and oxygen using electrical power, can be a carbon-free way to produce H_2 when coupled with renewable or nuclear energy sources. The integration of a sustainable energy source and water electrolysis is very attractive because of its high efficiency, close-to-zero emissions, and numerous applications (Fig. 1), although the cost is still higher than other conventional energy sources (*10*–*15*).

Compared to traditional water electrolysis technologies, proton exchange membrane electrolyzer cells (PEMECs) have several advantages, including a fast dynamic response time, a favorable energy efficiency/density, high hydrogen purity, and a more compact design (*16*–*18*). Although PEMECs have been in use for decades, there are still several significant challenges before they can be widely applied in hydrogen/oxygen production, including cost, durability, and efficiency (*17*, *19*–*21*). PEMECs use a proton exchange membrane (PEM) as the electrolyte, which permits proton transport from anode to cathode, and typically, $IrRuO_x$ and Pt/B are used as the anode and cathode catalysts, respectively. Two of the main cost drivers inhibiting more widespread PEMEC use are catalyst loading/catalyst use for the electrochemical reaction and degradation of materials and components, as a result of the electrochemical reaction (*22*–*29*).

The main purpose of a PEMEC is to electrochemically split water into hydrogen and oxygen. During the operation, as shown in fig. S1, water is circulated at the anode side through a flow field to the membrane electrode assembly (MEA), where it electrochemically reacts with the catalyst and is split into oxygen, protons, and electrons. The protons are then transported through the membrane, react with electrons from an external electrical force, and form hydrogen at the cathode, which exits through the flow channel at the cathode side. Meanwhile, the oxygen and water are transported out at the anode side.

The stoichiometric equations for the electrochemical reactions on both sides in a PEMEC are shown in Eqs. 1 and 2. Theoretically, the amount of gases produced per unit time is directly related to the current that passes through the electrochemical cell

$$\text{Anode}: \ 2H_2O \xrightarrow{\text{Catalyst}} 4H^+ + O_2 + 4e^- \quad (1)$$

$$\text{Cathode}: \ 4H^+ + 4e^- \xrightarrow{\text{Catalyst}} 2H_2 \quad (2)$$

The performance of PEMECs depends on the electrochemical reactions and the associated properties of the MEA, including catalyst use, membrane conductivities, catalyst layer (CL) activities, and liquid/gas diffusion layer (LGDL) structures (*30*–*33*). In PEMECs, the electrochemical reactions occur only on "triple-phase boundaries" (TPBs), meaning locations with electron conductors, active catalysts, proton carriers, and pathways for reactants/products. For instance, a water-splitting location at the anode needs (i) a pore to transport liquid water in and gaseous oxygen out, (ii) a catalyst and electron conductors for the reaction, and (iii) an electrolyte for proton transport (*34*–*38*). To improve performance and bring down costs, it is important to understand the fundamental principles and real operational dynamics situation of TPB electrochemical reactions in PEMECs, including microscale interfacial effects. However, this has been challenging because the catalyst/reaction sites are located on CLs behind the other components: The electrochemical reaction site on CLs is next to the center part of the PEM

[1]Department of Mechanical, Aerospace, and Biomedical Engineering, University of Tennessee (UT) Space Institute, UT, Knoxville, TN 37388, USA. [2]Oak Ridge National Laboratory, Oak Ridge, TN 37831, USA. [3]National Renewable Energy Laboratory, Golden, CO 80401, USA. [4]Department of Mechanical, Aerospace, and Biomedical Engineering, UT, Knoxville, TN 37996, USA.
*Corresponding author. Email: fzhang@utk.edu

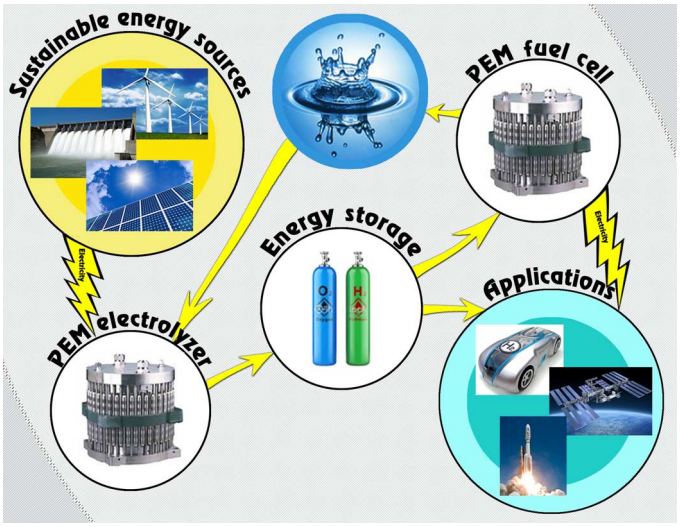

Fig. 1. Schematic of applications of PEMECs and PEM fuel cells coupled with sustainable energy sources.

and behind the LGDLs, current distributor with flow channel, and end plate. In addition, conventional microscopes will not meet observational needs at high spatial resolution because LGDLs are typically made of titanium fibers or foam with random interconnected and complicated pore morphology, current distributors are made from titanium to resist the high potential and oxidative environment, and a large working distance for optical systems is required. The electrochemical reactions are rapid and microscale. These factors have made it nearly impossible to perform in situ characterization to determine the role of the TPB and electrochemical reaction phenomena in PEMECs.

RESULTS

Here, we introduce a transparent and reaction-visible PEMEC, coupled with a high-speed and microscale visualization system (HMVS) and electrochemical impedance spectroscopy for electrochemical reaction quantification. With micro/nanotechnology and advanced manufacturing, thin LGDLs with throughout openings have been developed and implemented to permit direct visualization of the electrochemical reactions in the PEMEC. The true mechanisms of the rapid, microscale electrochemical reactions of splitting water in PEMECs have thus been revealed for the first time.

A typical image of electrochemical reactions in a PEMEC microchannel with high-speed, microscale visualizations is shown in Fig. 2A. The black parts in the channel are CLs, and the gray shiny areas are LGDLs, which appear between the gray dim parts—lands of the microchannel. The thin LGDL has uniform triangular opening distribution with an opening height of about 600 μm and an opening wall width of about 150 μm. During operation, the microchannel of the PEMEC was filled with deionized (DI) water and the PEMEC was operated with a constant current density. The cell voltage was around 2.5 V, under a current density of 2 A/cm^2 at room temperature, which is similar to a conventional cell (*39*).

Oxygen bubbles are formed on the surfaces of the CLs (black parts), which are adjacent to LGDLs (gray shiny parts). Then, because of electrochemical reactions and coalescence, they grow, detach from the CL surfaces, merge with each other, and finally flow out of the PEMEC with DI water through the microchannel. During this process, several types of liquid/gas two-phase flow are formed in the microchannel. More details with a typical video clip can be viewed in movie S1. Surprisingly, the reaction sites, where the oxygen bubbles are generated (confirmed/discussed later in Fig. 3D), have some preferences and did not uniformly occupy the CL surface. The oxygen bubbles appear to be generated only at the interface of the LGDL and CL. As shown in Fig. 2 (B to E), most of the bubbles are generated along the edge of the openings, even with different opening sizes (from 50 to 500 μm) and different opening shapes. Although some bubbles are observed in the middle of openings, they just flow with the flowing DI water after detaching from the CL.

The visualization results indicate that observable reactions occur almost exclusively along the CL-LGDL walls, as shown in Fig. 3A. Usually, CLs in PEMECs have been designed and fabricated as reaction sites to conduct electrons, protons, and reactants/products. Until now, it has been assumed that reactions occur across the entire CL surface (as shown in Fig. 3B), where they meet the conventional TPB requirements (as shown in Fig. 3C). To verify whether the bubble generation sites are the same as the electrochemical reaction sites, several experiments were designed and conducted to suppress the interfacial phenomena. As shown in Fig. 3D and movies S6 and S7, both electrically conductive wire (thin tungsten) and nonconductive wire (plastic microfiber) with similar diameters of about 50 μm were put across LGDLs on the CL surfaces. When the PEMEC was operating at a current density of 2 A/cm^2, there was bubble generation/nucleation only along the conductive wire, which can easily conduct electrons for electrochemical reactions. The two wires were put in several different locations, and the same phenomena were observed. This preclusive experiment further confirmed that the bubble generation/nucleation sites observed in this research are the sites of electrochemical reaction. This discovery presents a potential opportunity to enhance the multiphase interfacial reactions and significantly reduce the use of catalysts for commercial applications through heterogeneous distribution of catalysts along the CL-LGDL interfaces, as proposed in Fig. 3E.

To further confirm our findings on the basis of an operational PEMEC, we introduced a novel catalyst fabrication. As shown in Fig. 4A, the conventional method of catalyst fabrication is via directly spraying or brushing on the membrane. On the basis of our findings, it would appear that a lot of catalysts are wasted in the middle area of LGDL openings. To optimize catalyst use, we only sputter-coated the catalyst of thin Pt film on the LGDL, as shown in Fig. 4B. Through ex situ investigation of both CLs, the microstructures, which are quite different, are presented in scanning electron microscopy images (Fig. 4, C and D). The catalyst loaded on the membrane using conventional methods has a finer crystal structure than the catalyst sputter-coated on the LGDL, which could be one of the reasons that the PEMEC with the sputter coating catalyst has a worse performance. However, the performance results for this novel fabricated CL were very close to those for a conventionally fabricated CL (Fig. 4E). It is noteworthy that the thickness of the CL is reduced from 15 μm to 15 nm; thus, the mass activity of the catalyst with sputter coating on LGDL is far greater than that with the conventional method of loading platinum black (Pt/B) on the membrane (more than 54 times, as shown in Fig. 4F; see the Supplementary Materials for calculation details) (*40*). These results provide very strong support for the previously mentioned assumptions that the electrochemical reactions only occur on the CL locations that meet the TPB requirements and have good electron conductivities with small in-plane ohmic overpotential. A better electron conductor in $IrRuO_x$ CL will be needed to fulfill the expected electrochemical reactions.

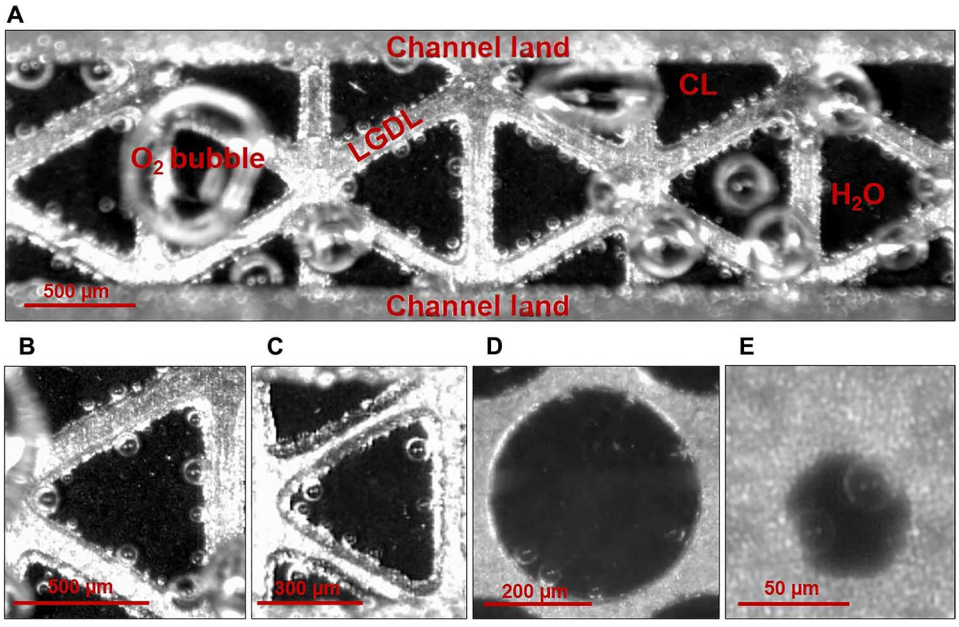

Fig. 2. Microscale electrochemical reactions in PEMECs. (**A**) Front-view image of electrochemical reactions in the PEMEC microchannel (movie S1). (**B**) Triangular opening (600 μm; movie S2). (**C**) Triangular opening (400 μm; movie S3). (**D**) Circular opening (500 μm; movie S4). (**E**) Circular opening (50 μm; movie S5).

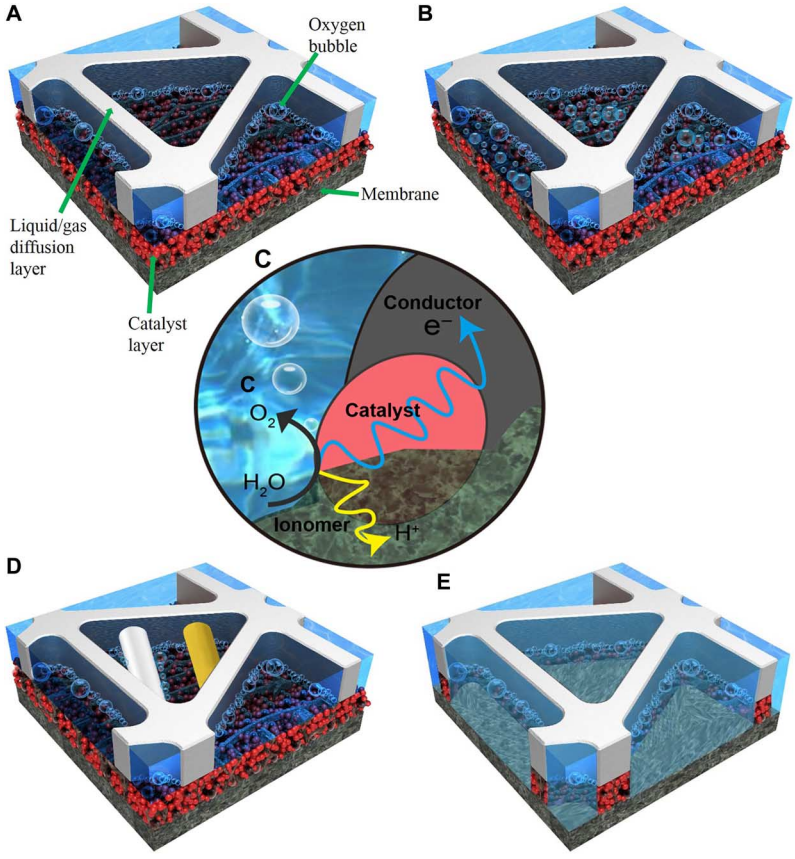

Fig. 3. Schematic of opening-scale electrochemical reactions occurring in the anode of a PEMEC. (**A**) True electrochemical reaction phenomena as revealed in this study. (**B**) Conventional perception of electrochemical reactions. (**C**) TPB electrochemical reaction. (**D**) Phenomena demonstrated in preclusive experiments described in this paper [white wire, thin tungsten wire as conductive material (movie S6); yellow wire, plastic microfiber as nonconductive material (movie S7)]. (**E**) Suggested future design for CLs in PEMECs: the catalyst is only deposited on the lands of LGDLs.

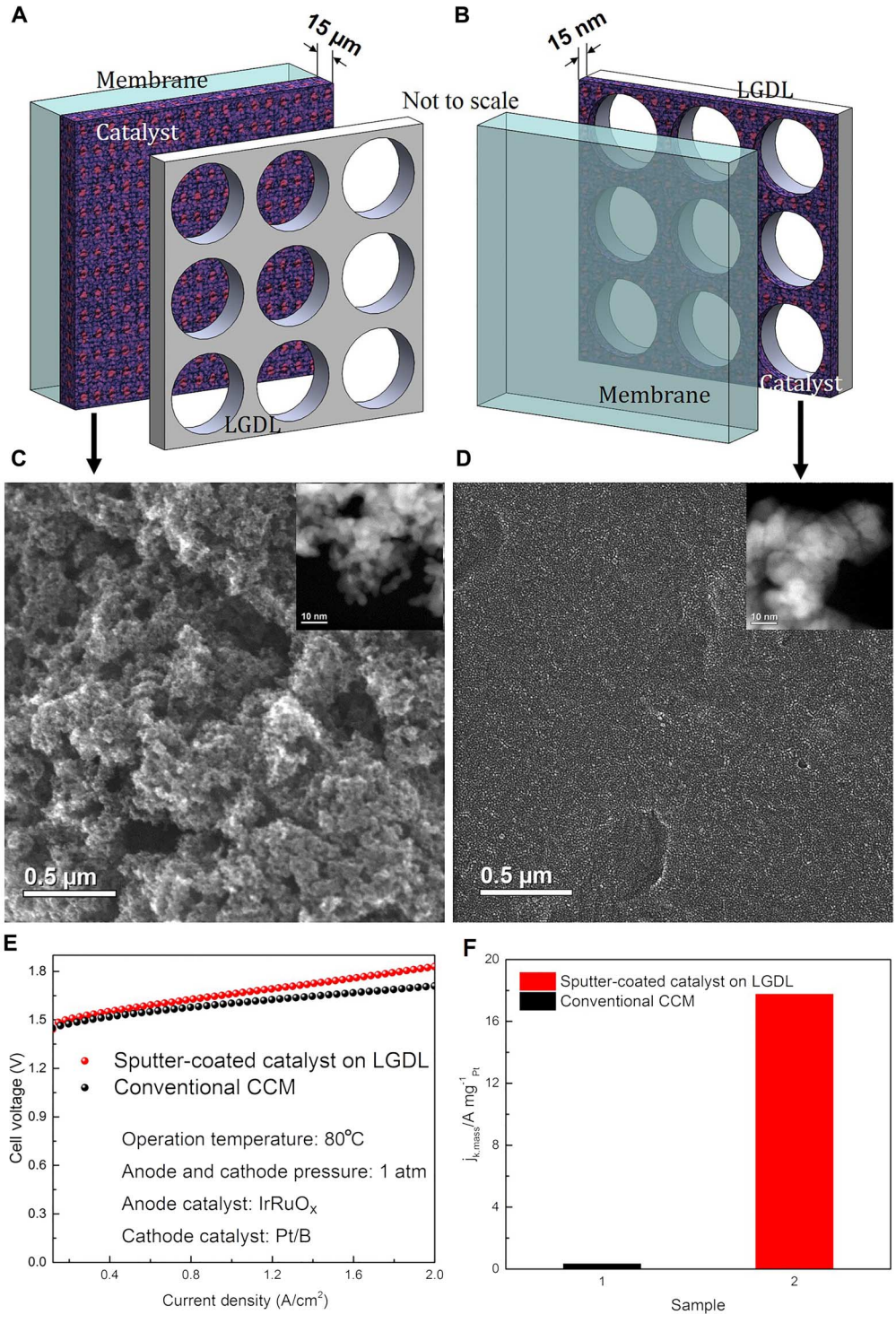

Fig. 4. Comparison of different catalyst loading methods and substrates in the cathode of a PEMEC (one is on the membrane and the other one is on the LGDL). (**A**) Schematic of an LGDL and a conventional catalyst-coated membrane (CCM). (**B**) Schematic of a catalyst sputter-coated on LGDL. (**C**) Secondary electron scanning transmission electron microscopy and high-angle annular dark-field scanning transmission electron microscopy (inset) images of a catalyst structure on a conventional CCM. (**D**) Secondary electron scanning transmission electron microscopy and high-angle annular dark-field scanning transmission electron microscopy (inset) images of a catalyst sputter-coated on LGDL. (**E**) Performance comparison of cells with a conventional CCM and a catalyst sputter-coated on LGDL. (**F**) Comparison of mass activities of the catalyst between a conventional CCM and a sputter-coated catalyst on LGDL.

DISCUSSION

The discovery described in this article challenges previous assumptions for PEMECs, that is, that electrochemical reactions should occur fairly uniformly over the entire surface of CL. To date, all commercial companies fabricate the CL with uniform distributions of catalysts and TPBs on the surface of membranes. However, the in situ visualization results indicate that electrochemical reactions do not occur in most TPBs, which means that the catalyst loaded on CLs (the most expensive part in the device) did not function as designed, representing a significant waste. The requirements for the electrochemical reaction not only include TPB conditions—pathways for reactants and products, active catalysts, and conductors for protons and electrons—but also require excellent electron conduction. It can be assumed that, in PEMECs, the water is only decomposed to protons, electrons, and oxygen at the locations with good electron conduction, where the TPB exists in the anode of the PEMEC. In the current situation, the electron conductor is a critical threshold for electrochemical reactions. Meanwhile, the in-plane ohmic resistivity of the $IrRuO_x$ CL has been found to be more than 10,000 times larger than the thin titanium LGDL. The large in-plane ohmic losses in CLs prevent the electrochemical reactions from occurring in the middle regions for even very small openings, as shown in Fig. 2E. The absence of electrochemical reactions in the region results in no oxygen bubble formation and growth, which, in turn, explains the phenomena observed in an operating PEMEC.

Our experiments revealed that the in situ electrochemical reaction behaviors in PEMECs could serve as a guide for improved fabrication and optimization of CLs, even PEMECs as a whole. For example, CLs might only be deposited on the edges of LGDLs, as shown in Fig. 3E. Modifications such as this could significantly reduce the use of expensive catalysts in PEMECs while maintaining performance levels, addressing the major barrier to the broad commercial application of PEMECs. Fundamental understandings from this research could also guide research to improve multiphase interfacial efficiency, increase catalyst efficiency, and promote the reaction areas of PEMECs and PEM fuel cells. In addition, controlled geometric LGDLs and cell architectures will enable more direct numerical simulations and validation through simplified and known internal morphology. Moreover, this research will open new possibilities to manipulate triple-phase interfacial effects in multiscale engineering devices, thus enabling innovative designs with novel control of capillary transport and rapid reactions for wide applications.

To thoroughly investigate electrochemical reaction locations in operating PEMECs, we developed a reaction-visible PEMEC consisting of a thin LGDL with straight openings and highly tunable morphology, and an HMVS. Surprisingly, reactions preferentially occur on the CL and LGDL interfaces, indicating that most of the catalysts loaded on CLs do not function as designed and are thus wasted. A preliminary result from the PEMEC with a novel fabricated CL has substantiated the visualization results and assumptions. Further understanding this real situation in nanoscale or crystallized scale will help to optimize CL and LGDL designs and fabrications, which will significantly reduce the use of expensive catalysts in PEMECs and speed up their wide commercialization as one of the most efficient ways of producing hydrogen and storing energy.

MATERIALS AND METHODS

A PEMEC mainly consists of a CCM sandwiched between two electrodes and two end plates, as shown in fig. S2. The CCM (Fuel Cells Etc Inc.) is a Nafion 115 film with $IrRuO_x$ (3.0 mg/cm^2) and Pt/B (3.0 mg/cm^2) used as anode and cathode catalysts, respectively. In the conventional PEMEC, both end plates are made of aluminum. The anode current distributor, with a parallel flow field, was fabricated from a titanium plate, whereas the cathode current distributor and flow field were fabricated from copper and graphite plate, respectively. The cathode gas diffusion layer was Toray 090 carbon paper treated with 5% polytetrafluoroethylene, whereas titanium felt was used as an anode LGDL. To visualize the electrochemical reactions in situ at the center of the PEMEC, we made some alterations compared to a conventional PEMEC. First, a rectangular hole was machined on the anode end plate as an observation window, which is similar to the transparent PEM fuel cell in our previous work (*41*–*43*). Second, the titanium anode current distributor with a parallel flow field was divided into two parts: a transparent plate with flow-in holes/channels and a 0.5 mm titanium plate with chemically etched parallel flow channels with a channel width of 1 mm. In addition, a novel thin anode LGDL was developed by using micro/nanofabrications on a thin titanium film with a thickness of 25 μm (*44*–*46*). The PEMEC with titanium thin anode LGDLs had shown much better performance than the one with standard titanium felt LGDLs in our previous research (*47*). Eight evenly distributed bolts were used to assemble the single 5 cm^2 cell with a torque of 40 lbf-in. The reaction-visible PEMEC was operated at room temperature with a flow rate of 40 ml/min controlled by a diaphragm liquid pump from KNF Neuberger.

In the PEMEC test, all electrochemical parameters were controlled by an SP-300 chassis with a 10 A/5 V booster kit. The built-in frequency response analyzer had a frequency range of 10 μHz up to 7 MHz. Galvanostatic electrochemical impedance spectroscopy was used to measure the impedance of the PEMEC under different operating conditions.

The HMVS is also unique and includes a high-speed camera (Phantom v711) and in-house optical assembly. The high-speed camera can achieve a maximum speed of 7500 frames per second (fps) at full resolution. At reduced resolutions, it can deliver up to 1,400,000 fps. The in-house optical assembly consists of a main zoom lens body and a series of objective and eyepiece lenses, with a working distance of >70 mm even at high resolution. This feature distinguishes it from a conventional microscope, which requires a much smaller working distance at a similar spatial resolution.

All aforementioned parts were fastened on XYZ stages and positioners with well-designed layout and control. The relative distance between the observation window of the reaction-visible PEMEC and HMVS could be finely regulated. In addition, a cold light source with adjustable intensity was introduced to this system through goosenecks to ensure high-quality videos and images. Local reaction activities could be monitored and analyzed on the basis of microscale oxygen production in reaction-visible/operational PEMECs by HMVS.

The electrical resistivity of materials for TPB reaction in PEMEC was measured. The thin film materials were measured with a four-point probe (Lucas Lab Pro 4-4400). Because the CL is a porous medium, there were some measurement fluctuations when the four-point probe was used; the value was the average of five measurements.

Nanomanufacturing of thin, highly tunable titanium LGDLs

To obtain the visual image from inside the PEMEC, we conducted some design modifications on a conventional electrolyzer. A novel thin anode LGDL was developed by using nanofabrications on a thin titanium film.

As shown in fig. S3, a low-cost wet etching process was specifically developed in the Oak Ridge National Laboratory (ORNL). The thin, highly tunable titanium LGDLs were manufactured using lithographically patterned resist masks and chemical wet etching of thin foils (*46*). The fabrication procedure for the titanium thin LGDL began with the design and fabrication of the photomasks. With this step, different opening sizes, opening shapes, and opening distributions can be achieved.

A mask pattern was designed using commercially available CAD/VLSI software (LayoutEditor; layouteditor.net). The design pattern was imported into a Heidelberg DWL 66 laser lithography system and patterned on a soda-lime glass mask plate that was precoated with chromium and a photoresist. After patterning, the masks were developed for 1 min in Microposit MF CD-26 Developer (Shipley Company), rinsed with DI water, and dried with N_2. Masks were then submerged in chrome etchant for 2 min, rinsed with DI water, and dried with N_2. The remaining resist was subsequently removed in a heated bath (70°C) of *N*-methylpyrrolidone. Masks were rinsed with DI water and dried with N_2. As shown in Fig. 2, to provide structural integrity of the extremely thin titanium foil, we affixed foils to a silicon wafer during processing. Substrate was treated with MicroPrime P20 Primer (Shin-Etsu MicroSi Inc.) adhesion promoter by coating the substrate with adhesion promoter, waiting for 10 s, and spin-drying the samples at 3000 rpm for 45 s. Subsequently, Microposit SPR220 photoresist (Rohm and Haas) was spin-coated onto samples at 3000 rpm for 45 s. The titanium film was then placed on the resist-coated silicon wafer with special care because of its delicate features and soft-baked for 90 s at 115°C. A second layer of P20 and SPR220 photoresist was applied to the titanium foil under identical conditions and then exposed to ultraviolet light using conventional contact photolithography. Masks were developed in Microposit MF CD-26 Developer (Shipley Company), rinsed with DI water, and dried with N_2. Finally, after patterning the photoresist mask on the foil, the patterned material was etched in hydrogen fluoride etchant. Thin, highly tunable titanium LGDLs with different opening sizes and opening shapes were fabricated.

SUPPLEMENTARY MATERIALS

Supplementary material for this article is available at http://advances.sciencemag.org/cgi/content/full/2/11/e1600690/DC1

Sequence of photos of electrochemical reactions in PEMEC micro-openings

Preliminary results for the new catalyst fabrication method

fig. S1. Schematic of a PEMEC.

fig. S2. Schematic of the transparent, reaction-visible PEMEC and LGDLs with highly tunable and straight holes throughout.

fig. S3. Schematic of a developed nanofabrication process for the titanium thin LGDL with highly tunable micro-openings.

fig. S4. A sequence images of electrochemical reactions in a triangle micro-opening of the thin, highly tunable titanium LGDL.

movie S1. Phenomena of electrochemical reaction occurring at microchannel scale (operation current density, 2 A/cm^2; DI water flow rate, 20 ml/min; channel size, 1 mm height; triangle opening size, 600 μm; duration, 0.058 s).

movie S2. Phenomena of electrochemical reaction occurring at micro-opening scale (operation current density, 2 A/cm^2; DI water flow rate, 20 ml/min; triangular opening size, 600 μm; duration, 0.058 s).

movie S3. Phenomena of electrochemical reaction occurring at micro-opening scale (operation current density, 2 A/cm^2; DI water flow rate, 20 ml/min; triangular opening size, 400 μm; duration, 0.069 s).

movie S4. Phenomena of electrochemical reaction occurring at micro-opening scale (operation current density, 2 A/cm^2; DI water flow rate, 20 ml/min; circular opening size, 500 μm; duration, 0.121 s).

movie S5. Phenomena of electrochemical reaction occurring at micro-opening scale (operation current density, 2 A/cm^2; DI water flow rate, 20 ml/min; circular opening size, 50 μm; duration, 0.112 s).

movie S6. Phenomena of electrochemical reaction occurring in a triangle opening with a thin tungsten wire as conductive wire (operation current density, 2 A/cm^2; DI water flow rate, 20 ml/min; triangular opening size, 600 μm).

movie S7. Phenomena of electrochemical reaction occurring in a triangle opening with a plastic microfiber as nonconductive wire (operation current density, 2 A/cm^2; DI water flow rate, 20 ml/min; triangular opening size, 600 μm).

REFERENCES AND NOTES

1. W. E. Winsche, K. C. Hoffman, F. J. Salzano, Hydrogen: Its future role in the nation's energy economy. *Science* **180**, 1325–1332 (1973).
2. T. N. Veziroglu, F. Barbir, Solar–hydrogen energy system: The choice of the future. *Environ. Conserv.* **18**, 304–312 (1991).
3. J. A. Turner, Sustainable hydrogen production. *Science* **305**, 972–974 (2004).
4. N. S. Lewis, Research opportunities to advance solar energy utilization. *Science* **351**, aad1920 (2016).
5. H. A. Gasteiger, N. M. Markovic, Just a dream—Or future reality? *Science* **324**, 48–49 (2009).
6. D. V. Esposito, S. T. Hunt, Y. C. Kimmel, J. G. Chen, A new class of electrocatalysts for hydrogen production from water electrolysis: Metal monolayers supported on low-cost transition metal carbides. *J. Am. Chem. Soc.* **134**, 3025–3033 (2012).
7. J. A. Turner, A nickel finish protects silicon photoanodes for water splitting. *Science* **342**, 811–812 (2013).
8. J. A. Turner, A realizable renewable energy future. *Science* **285**, 687–689 (1999).
9. N. S. Lewis, D. G. Nocera, Powering the planet: Chemical challenges in solar energy utilization. *Proc. Natl. Acad. Sci. U.S.A.* **103**, 15729–15735 (2006).
10. B. Rausch, M. D. Symes, G. Chisholm, L. Cronin, Decoupled catalytic hydrogen evolution from a molecular metal oxide redox mediator in water splitting. *Science* **345**, 1326–1330 (2014).
11. M. M. Mench, *Fuel Cell Engines* (John Wiley & Sons, 2008), 528 pp.
12. A. Marshall, B. Børresen, G. Hagen, M. Tsypkin, R. Tunold, Hydrogen production by advanced proton exchange membrane (PEM) water electrolysers—Reduced energy consumption by improved electrocatalysis. *Energy* **32**, 431–436 (2007).
13. F. Barbir, PEM electrolysis for production of hydrogen from renewable energy sources. *Sol. Energy* **78**, 661–669 (2005).
14. M. M. Mench, F.-Y. Zhang, Fuel Cells, in *Mechanical Engineers' Handbook*, vol. IV, *Energy and Power*, part 2, *Power* (John Wiley & Sons, 2015), chap. 31, pp. 1–34.
15. M. I. Hoffert, K. Caldeira, G. Benford, D. R. Criswell, C. Green, H. Herzog, A. K. Jain, H. S. Kheshgi, K. S. Lackner, J. S. Lewis, H. D. Lightfoot, W. Manheimer, J. C. Mankins, M. E. Mauel, L. J. Perkins, M. E. Schlesinger, T. Volk, T. M. L. Wigley, Advanced technology paths to global climate stability: Energy for a greenhouse planet. *Science* **298**, 981–987 (2002).
16. B. Han, S. M. Steen III, J. Mo, F.-Y. Zhang, Electrochemical performance modeling of a proton exchange membrane electrolyzer cell for hydrogen energy. *Int. J. Hydrogen Energy* **40**, 7006–7016 (2015).
17. M. Carmo, D. L. Fritz, J. Merge, D. Stolten, A comprehensive review on PEM water electrolysis. *Int. J. Hydrogen Energy* **38**, 4901–4934 (2013).
18. O. Khaselev, A. Bansal, J. A. Turner, High-efficiency integrated multijunction photovoltaic/electrolysis systems for hydrogen production. *Int. J. Hydrogen Energy* **26**, 127–132 (2001).
19. T. J. Toops, M. P. Brady, F. Y. Zhang, H. M. Meyer III, K. Ayers, A. Roemer, L. Dalton, Evaluation of nitrided titanium separator plates for proton exchange membrane electrolyzer cells. *J. Power Sources* **272**, 954–960 (2014).
20. J. Mo, S. M. Steen III, F.-Y. Zhang, T. J. Toops, M. P. Brady, J. B. Green Jr., Electrochemical investigation of stainless steel corrosion in a proton exchange membrane electrolyzer cell. *Int. J. Hydrogen Energy* **40**, 12506–12511 (2015).
21. A. Le Goff, V. Artero, B. Jousselme, P. D. Tran, N. Guillet, R. Métayé, A. Fihri, S. Palacin, M. Fontecave, From hydrogenases to noble metal–free catalytic nanomaterials for H_2 production and uptake. *Science* **326**, 1384–1387 (2009).
22. W. Xu, K. Scott, S. Basu, Performance of a high temperature polymer electrolyte membrane water electrolyser. *J. Power Sources* **196**, 8918–8924 (2011).
23. A. Stoyanova, G. Borisov, E. Lefterova, E. Slavcheva, Oxygen evolution on Ebonex-supported Pt-based binary compounds in PEM water electrolysis. *Int. J. Hydrogen Energy* **37**, 16515–16521 (2012).
24. R. Tunold, A. Marshall, E. Rastenc, M. Tsypkin, L.-E. Owe, S. Sunde, Materials for electrocatalysis of oxygen evolution process in PEM water electrolysis cells. *ECS Trans.* **25**, 103–117 (2010).
25. H. H. Hwu, J. G. G. Chen, Surface chemistry of transition metal carbides. *Chem. Rev.* **105**, 185–212 (2005).
26. J. Suntivich, H. A. Gasteiger, N. Yabuuchi, H. Nakanishi, J. B. Goodenough, Y. Shao-Horn, Design principles for oxygen-reduction activity on perovskite oxide catalysts for fuel cells and metal–air batteries. *Nat. Chem.* **3**, 546–550 (2011).
27. M. K. Debe, S. M. Hendricks, G. D. Vernstrom, M. Meyers, M. Brostrom, M. Stephens, Q. Chan, J. Willey, M. Hamden, C. K. Mittelsteadt, C. B. Capuano, K. E. Ayers, E. B. Anderson, Initial performance and durability of ultra-low loaded NSTF electrodes for PEM electrolyzers. *J. Electrochem. Soc.* **159**, K165–K176 (2012).
28. K. E. Ayers, E. B. Anderson, C. B. Capuano, B. D. Carter, L. T. Dalton, G. Hanlon, J. Manco, M. Niedzwiecki, Research advances towards low cost, high efficiency PEM electrolysis. *ECS Trans.* **33**, 3–15 (2010).
29. K. E. Ayers, J. N. Renner, N. Danilovic, J. X. Wang, Y. Zhang, R. Maric, H. Yu, Pathways to ultra-low platinum group metal catalyst loading in proton exchange membrane electrolyzers. *Catal. Today* **262**, 121–132 (2016).
30. S. Song, H. Zhang, X. Ma, Z. Shao, R. T. Baker, B. Yi, Electrochemical investigation of electrocatalysts for the oxygen evolution reaction in PEM water electrolyzers. *Int. J. Hydrogen Energy* **33**, 4955–4961 (2008).

31. L. Ma, S. Sui, Y. Zhai, Investigations on high performance proton exchange membrane water electrolyzer. *Int. J. Hydrogen Energy* **34**, 678–684 (2009).
32. C. Y. Du, P. F. Shi, X. Q. Cheng, G. P. Yin, Effective protonic and electronic conductivity of the catalyst layers in proton exchange membrane fuel cells. *Electrochem. Commun.* **6**, 435–440 (2004).
33. J. Shui, M. Wang, F. Du, L. Dai, N-doped carbon nanomaterials are durable catalysts for oxygen reduction reaction in acidic fuel cells. *Sci. Adv.* **1**, e1400129 (2015).
34. H. Zhang, G. Lin, J. Chen, Evaluation and calculation on the efficiency of a water electrolysis system for hydrogen production. *Int. J. Hydrogen Energy* **35**, 10851–10858 (2010).
35. R. O'Hayre, F. B. Prinz, The air/platinum/Nafion triple-phase boundary: Characteristics, scaling, and implications for fuel cells. *J. Electrochem. Soc.* **151**, A756–A762 (2004).
36. R. P. Iczkowski, M. B. Cutlip, Voltage losses in fuel cell cathodes. *J. Electrochem. Soc.* **127**, 1433–1440 (1980).
37. J. Suntivich, K. J. May, H. A. Gasteiger, J. B. Goodenough, Y. Shao-Horn, A perovskite oxide optimized for oxygen evolution catalysis from molecular orbital principles. *Science* **334**, 1383–1385 (2011).
38. K. Gong, F. Du, Z. Xia, M. Durstock, L. Dai, Nitrogen-doped carbon nanotube arrays with high electrocatalytic activity for oxygen reduction. *Science* **323**, 760–764 (2009).
39. S. A. Grigoriev, V. I. Porembsky, V. N. Fateev, Pure hydrogen production by PEM electrolysis for hydrogen energy. *Int. J. Hydrogen Energy* **31**, 171–175 (2006).
40. L. Zhang, L. T. Roling, X. Wang, M. Vara, M. Chi, J. Liu, S.-I. Choi, J. Park, J. A. Herron, Z. Xie, Platinum-based nanocages with subnanometer-thick walls and well-defined, controllable facets. *Science* **349**, 412–416 (2015).
41. F.-Y. Zhang, D. Spernjak, A. K. Prasad, S. G. Advani, In situ characterization of the catalyst layer in a polymer electrolyte membrane fuel cell. *J. Electrochem. Soc.* **154**, B1152–B1157 (2007).
42. F.-Y. Zhang, X. G. Yang, C. Y. Wang, Liquid water removal from a polymer electrolyte fuel cell. *J. Electrochem. Soc.* **153**, A225–A232 (2006).
43. X. G. Yang, F.-Y. Zhang, A. L. Lubawy, C. Y. Wang, Visualization of liquid water transport in a PEFC. *Electrochem. Solid St.* **7**, A408–A411 (2004).
44. F.-Y. Zhang, A. K. Prasad, S. G. Advani, Investigation of a copper etching technique to fabricate metallic gas diffusion media. *J. Micromech. Microeng.* **16**, N23 (2006).
45. F.-Y. Zhang, S. G. Advani, A. K. Prasad, Performance of a metallic gas diffusion layer for PEM fuel cells. *J. Power Sources* **176**, 293–298 (2008).
46. J. Mo, S. M. Steen III, S. Retterer, D. A. Cullen, A. Terekhov, F.-Y. Zhang, Mask-patterned wet etching of thin titanium liquid/gas diffusion layers for a PEMEC. *ECS Trans.* **66**, 3–10 (2015).
47. J. Mo, Z. Kang, G. Yang, S. T. Retterer, D. A. Cullen, T. J. Toops, J. B. Green Jr., F.-Y. Zhang, Thin liquid/gas diffusion layers for high-effieciency hydrogen production from water splitting. *Appl. Energy* **177**, 817–822 (2016).

Acknowledgments: We wish to express our appreciation to B. Han, S. Steen, G. Yang, W. Barnhill, A. Terekhov, D. Warnberg, R. Chen, and N. Kaptur for their help. **Funding:** Financial support for this study was provided by the U.S. Department of Energy's (DOE) National Energy Technology Laboratory under award DE-FE0011585. The research was partially performed at ORNL's Center for Nanophase Materials Sciences, which is sponsored by the DOE Office of Basic Energy Sciences.
Author contributions: F.-Y.Z., M.M.M., and J.M. contributed to the design of the study. F.-Y.Z. and J.M. organized the research project. J.M., Z.K., S.T.R., D.A.C., and F.-Y.Z. conducted the experiments and data analysis. T.J.T. and J.B.G. provided technical support, conceptual advice, and result interpretation. J.M. drafted the main paper. All authors commented on and edited the manuscript. **Competing interests:** The authors declare that they have no competing interests. **Data and materials availability:** All data needed to evaluate the conclusions in the paper are present in the paper and/or the Supplementary Materials. Additional data related to this paper may be requested from the authors.

Submitted 31 March 2016
Accepted 29 September 2016
Published 18 November 2016
10.1126/sciadv.1600690

Citation: J. Mo, Z. Kang, S. T. Retterer, D. A. Cullen, T. J. Toops, J. B. Green, M. M. Mench, F.-Y. Zhang, Discovery of true electrochemical reactions for ultrahigh catalyst mass activity in water splitting. *Sci. Adv.* **2**, e1600690 (2016).